Nanoscale

ROYAL SOCIETY
OF CHEMISTRY

PAPER
Yi Huang *et al.*
Facile fabrication of zeolitic imidazolate framework hollow
fibre membranes *via* a novel scalable continuous fluid
circulation process

NCNST

Nanoscale

PAPER

Check for updates

Facile fabrication of zeolitic imidazolate framework hollow fibre membranes *via* a novel scalable continuous fluid circulation process†

Allana Lewis, Ting Chen, Fraz Saeed Butt, Xiuming Wei, Norbert Radacsi, [ID] Xianfeng Fan and Yi Huang [ID] *

A novel continuous fluid circulation system was designed and employed for the impregnation seeding and fabrication of zeolitic imidazolate framework (ZIF) crystals on the internal surface of polymeric hollow fibre membranes. Application of impregnation seeding has been proven effective to decrease crystal size, consequently increasing surface roughness and wettability of the membrane. Evaluation of the as-synthesised membrane demonstrated excellent separation efficiencies (>99%) of surfactant stabilised oil-in-water emulsions. Owing to the simple impregnation strategy assisted by the continuous fluid circulation, the active ZIF layer formed was visibly thinner and denser than typical seeding techniques, hence a high pure water flux of >1150 L m^{-2} h^{-1} bar^{-1} was achieved. The membranes were highly selective and ultra-permeable to water, however, almost impermeable to oils in a water environment, *e.g.*, *n*-hexane, *n*-heptane, chloroform and dichloromethane, as well as their emulsion mixtures, with a separation efficiency higher than 99%. Besides, this new continuous fluid circulation method was also found promising for the synthesis of other types of ZIF on hollow fibre membranes.

Introduction

Oil/water separations have received extensive attention in recent years due to an increased volume of discharged oily wastewater.[1–3] More specifically, emulsified oil-in-water mixtures have aroused great interest owing to their complex separation properties and the presence of surfactants – used for kinetic stabilisation of the mixture.[4] The application of surfactant-stabilised emulsions are commonly encountered in numerous industrial practices, for example, oil refinery, food, cosmetics and pharmaceuticals, as well as being a by-product in many manufacturing processes, such as wood and metal processing.[5–8] Emulsion pollution has reported an increase in biochemical oxygen demand (BOD) in the environment. However, these toxic chemicals not only pose a serious threat to maintaining a sustainable aquatic ecosystem but also cause unprecedented harms to human beings.[9] Therefore, an effective separation technique for oil removal from complex emulsified mixtures is necessary.

Demulsification has previously been achieved by numerous separation techniques such as electro-flotation,[10] electrocoagulation[9] and gravity settling. However, these methods typically suffer from low separation efficiency (limited efficiency for oil droplets <20 μm) and high operational costs.[11–14] Comparatively, membranes have demonstrated excellent separation efficiency due to their highly selective nanostructures and optimised surface properties.[14–16] Furthermore, membrane separations have been considered advantageous over the above-mentioned traditional techniques as they withhold a relatively small carbon footprint with low-energy and simple operation.[17–19] In regards to oil/water mixtures, separation efficiency is usually optimised by exploiting the membrane surface wettability to achieve the selective removal of oil molecules from the aqueous phase.[20–24] Besides, the specific membrane surface area is considered crucial for separation performance, improving the availability of interactive sites on the surface.[25–27] To satisfy these unique demands, membrane functionalisation with carboxyl, hydroxyl or amino groups or membrane decoration with various nanomaterials such as metal–organic frameworks (MOFs) have been shown to be effective on surface modification.[28,29] For instance, membranes with zeolitic imidazole frameworks (ZIFs), a subclass of MOFs, are considered promising candidates for many challen-

*School of Engineering, Institute for Materials and Processes, University of Edinburgh, Robert Stevenson Road, Edinburgh, EH9 3FB Scotland, UK.
E-mail: Yi.Huang@ed.ac.uk*

†Electronic supplementary information (ESI) available: Preparation (using different seeding and secondary fabrication techniques), characterisations (SEM, XRD and kinetic contact angle measurements) and oil/water separation performance of hollow fibre supported ZIF membranes. See DOI: 10.1039/d1nr03112k

ging mixture separations due to their tunable pore structure and excellent stability.[30] In the recent decade, ZIF membranes have been successfully prepared *via* seeding-secondary growth,[31] dip coating,[32] electrospinning,[33] and 3D printing approaches.[34] However, they usually require either a long synthesis procedure at elevated temperatures or produce high levels of waste.[34–38] Therefore, fast and simple protocols for more sustainable synthesis of highly selective and permeable ZIF membranes for water remediation is still highly demanded. In recent years, ZIFs has been applied to various supports such as metallic meshes, nanofibre supports, flat sheet polymeric and ceramic membranes.[39–42] Interestingly, very limited research has been reported for the fabrication of ZIFs on hollow fibre membranes despite their advantageous high surface area per volume ratio and great potential in scaling up production.[43–45] Herein, a novel continuous fluid circulation (CFC) fabrication method is introduced and, for the first time, applied for the facile fabrication of hollow fibre supported ZIF membranes (HF-ZifMs) with a significant reduction in waste production. The efficiency of this fabrication method in ZIF membrane formation was also examined. As mentioned above, demulsification of oil-in-water emulsions is challenging but significant for oily wastewater treatment, especially for surfactant-stabilised oil-in-water (s-O/W) emulsions. In this work, the performance of HF-ZifMs on continuous oil removal from s-O/W emulsions and their long-term stabilities in harsh conditions were thus systematically studied.

Experimental

Materials

Modified Polyethersulfone (PES) hollow fibre membranes (500 nm pore size) were obtained from NX Filtration B.V. 2-Methylimidazole (Hmim; 99%) and Zinc nitrate hexahydrate (Zn(NO$_3$)$_2$·6H$_2$O; 98%) were purchased from Sigma-Aldrich

Company Ltd, and Alfa Aesar, respectively. Emulsion surfactant – Tween 80 was also purchased from Sigma Aldrich. Chloroform (99.8%), *n*-hexane (99%), and *n*-heptane (99%) were purchased from Alfa Aesar. All other solvents, including ethanol (99.8%) and all other oils used in the oil/water separation experiments, were supplied by Fisher Scientific UK Ltd and were used as received. Sodium hydroxide (>97%) and hydrochloric acid (35%) for stability analyses were purchased from Merck and Sigma-Aldrich, respectively.

Fabrication of ZIF-L coated hollow fibres

The hollow fibre supports (~10 cm × ⌀ 2.5 mm) first underwent a gentle cleaning in deionised water for 24 hours and then oven-dried at 60 °C prior to subsequent fabrications. The fabrications were carried out using a simple pre-seeding or impregnation technique followed by a secondary growth process. ZIF-L aqueous synthesis solutions were prepared as 55 mM Zn (NO$_3$)$_2$·6H$_2$O$_{(aq)}$ and 390 mM 2-methylimidazole$_{(aq)}$ (V : V = 1 : 1) in accordance to our previous study.[46] Systematic adaptations were made to optimise the fabrications and separation performance tests (Fig. 1), including the use of ethanol during ZIF-L membrane fabrication (more details in ESI†). All four fabrication approaches were carried out in a homemade continuous fluid circulation system at a flow rate of 1 mL min^{-1} (Fig. 2). The as-synthesized HF-ZifMs were rinsed thoroughly with deionised water and dried vertically at room temperature.

Oil-in-water emulsion separation

Surfactant stabilised oil-in-water emulsions were prepared with 1 mL of cyclohexane in 99 mL of deionised water to form a 1% mixture following a previously published work.[47] The oil, water and surfactant mixture was vigorously stirred prior to sonication at 140% power (Model; US-CU-CA3L; 220–240 V (50 Hz), 40 kHz Frequency, 100 W Ultrasonic and Heating Power) for a minimum of 2 hours. The oil droplets have an average particle size of 2.7 ± 0.5 µm.
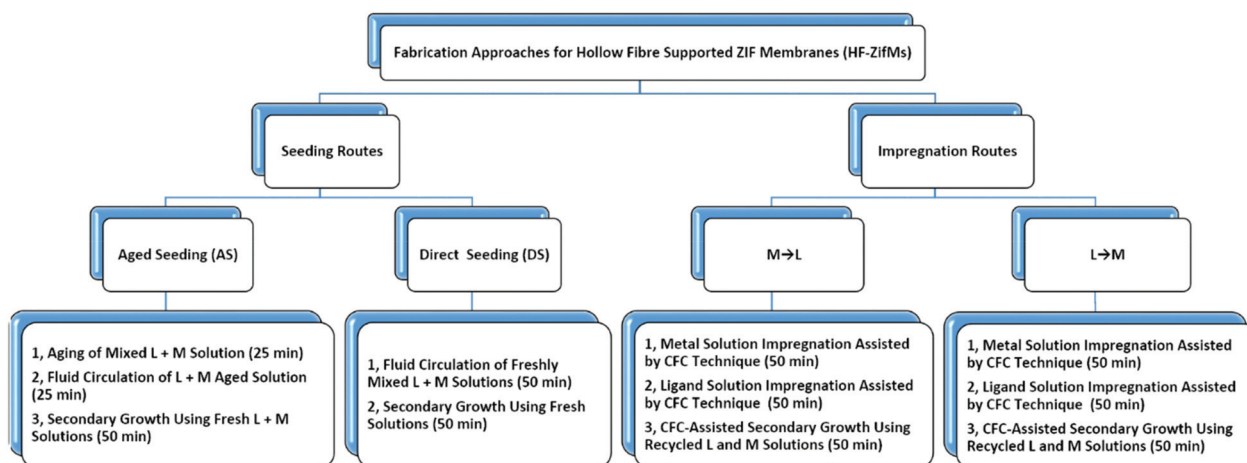

Fig. 1 Flow diagram of systematically studied approaches for the fabrication of hollow fibre supported ZIF membranes (HF-ZifMs). L and M denote ligand and metal solutions, respectively. M → L denotes metal solution was circulated first during the fabrication, followed by ligand solution. CFC denotes continuous fluid circulation.
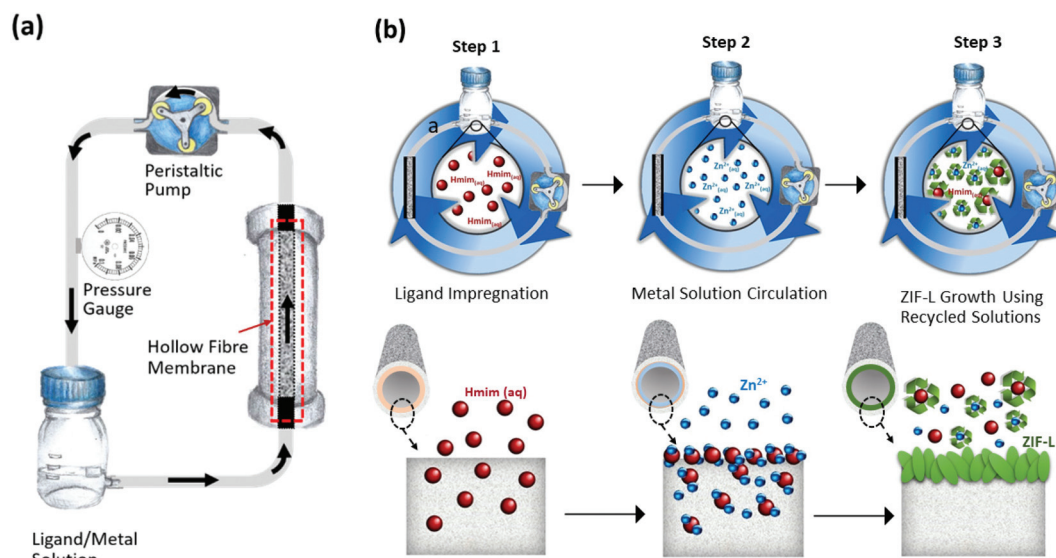
Fig. 2 (a) A homemade continuous fluid circulation (CFC) system; (b) schematic illustration of fabrication mechanism of HF–ZifMs *via* CFC technique.

The separation tests, oil removal from s-O/W emulsions, were carried out in a cyclic tubular membrane crossflow system with a Kronos 50 peristaltic pump drive and an SS316 membrane module type PVM-025–1 (Videos S1 and S2, ESI†). The effective surface area was then determined based upon the length (H) and the radius of the hollow fibre (r). Prewetting of the membranes was complete prior to emulsion separations by flushing the system with deionised water. Membrane permeation flux (L m^{-2} h^{-1} bar^{-1}) was calculated using eqn (1) after membrane stabilisation.

$$F = \frac{V}{S\Delta P\Delta T} \quad (1)$$

where V is the volume of permeate (L), S is the effective filtration area (m^2), ΔT is the permeation time (h) and ΔP is the pressure (bar). Pure water flux (F') was also calculated using eqn (1). The permeate volume was determined as water permeated through the hollow fibre membranes from the internal to the external surface. Real-time flux in 1-minute increments was evaluated for pure water permeation tests for a period of 2 h and 0.5 h for oil-in-water emulsion tests.

The separation efficiency of the membrane was calculated based upon the total organic carbon concentration of both the emulsion and permeate comparatively using eqn (2).

$$R = \left(1 - \frac{C_p}{C_f}\right) \times 100\% \quad (2)$$

where R represents the separation efficiency (%), C_p is the permeate concentration, and C_f is the feed solution concentration in mg L^{-1}. Despite the challenging separation of surfactants from water, the separations demonstrated a much lower total organic carbon than presented in the surfactant solution. Therefore, the results herein are representative of the extreme

scenarios, assuming that the carbon present in the permeate is due to oil presence rather than surfactants.

Characterisation

Internal surfaces and cross-section of the HF–ZifMs were observed using a scanning electron microscope (SEM JEOS JSM-IT100). All SEM samples were attained by freezing with liquid nitrogen and breaking. Each sample was sputter-coated with ~10 nm gold layer prior to analysis. The crystalline structure of the as-synthesised material, obtained from flat sheet equivalent membranes, was analysed by X-ray diffraction (XRD, Bruker D8 Advance) with Cu Kα radiation in a 2θ range of 5.0°–40.0°. Water and oil contact angles were analysed using Ossila Contact Angle equipment and software. Oil concentration was determined for both feed and filtrate of emulsion samples using total organic carbon content analysis (Shimadzu TOC-V). Visual representations of emulsion feed and filtrate were collected using bright field focal microscopy (Leica Epifluorescence Microscope).

Results and discussion

Fabrication of hollow fibre supported ZIF-L membranes

The HF–ZifMs were fabricated using a simple impregnation and secondary growth technique *via* a continuous fluid circulation (CFC) system at room temperature (Fig. 2a). The CFC method allowed the circulation of independent ligand and metal solutions through the hollow fibre, forming a gel-like film containing ZIF nuclei at the liquid–membrane interface. After seeding, a secondary growth was initiated by mixing the two recycled solutions together to induce crystal formation at the surface of the hollow fibre (Fig. 2b). In order to optimise this CFC system, a systematic study was investigated in terms

of seeding and growth techniques of ZIF crystals on hollow fibre support. This included four different fabrication approaches; an aged seeding (AS) technique which is used in many ZIF fabrications, a direct seeding (DS) technique and two impregnation techniques of the independent solutions (L → M and M → L) (see more details of different seeding techniques in the ESI†).

The AS approach fabricated a ZIF-L coating on the hollow fibre inner surface using a traditional seeding and secondary growth technique, as reported earlier.[48] In this method, a seeding solution was prepared by mixing 55 mM $Zn(NO_3)_2 \cdot 6H_2O$ (aq) and 390 mM 2-methylimidazole (aq) (V : V = 1 : 1). The seeding solution was stirred for 25 minutes and then used as a continuously circulated feed in the CFC system for 25 minutes at room temperature to complete the seeding process. After the initial seeding, the bare hollow fibre skeleton was covered by a thin layer of ZIF-L seeds (Fig. 3a). The crystal growth was promoted during secondary growth in a new solution prepared by mixing the fresh ligand and metal solutions. After 50 minutes of continuous circulation of the freshly prepared solution, the membrane synthesis was stopped and the as-synthesised membrane was thoroughly washed with deionised water. As shown in Fig. 3a–c, the hollow fibre was fully covered with randomly oriented ZIF-L crystals, displaying a very rough surface.

Interestingly, the morphology of the crystals was found to be significantly influenced by the seeding method applied. In this study, impregnation of independent ligand and metal solutions (L → M approach) gives promising morphological analysis whilst overcoming the challenges of the seeded membranes. In regards to a traditional seeding technique (AS/DS), a dense layer and non-uniform growth on hollow fibre surfaces occur. Comparatively, a thinner active layer with greater uniformity of ZIF-L crystals can be observed by our CFC impregnation system, which is highly advantageous to separation processes. Furthermore, the recycling of the impregnation solutions results in a 50% decrease in waste materials, using a total of 80 mL in comparison to the 160 mL used in traditional seeding techniques. Overall, this facile fabrication process requires a shorter growth time than comparable membranes and achieves a greener practice; reduced volumes of waste, use of green solvents (ethanol and water) and low energy fabrication (ambient condition fabrications).

Morphological analysis

The morphological analysis of the surface material, including surface morphology and cross-sectional analysis, was characterised using SEM imaging for both the conventional seeding method and the CFC method (Fig. 3). Images were recorded after seeding/CFC-assisted impregnation and a 50-minute continuous fluid circulation secondary growth to highlight the morphological changes in comparison to bare hollow fibres.

Previous works on membrane synthesis have emphasised the importance of the seeding technique to grow uniform ZIF-L on the support surface.[49–51] In this work, the effect of the seeding techniques on subsequent membrane growth was systematically studied using a home-made CFC system and a commercial polyamide hollow fibre membrane support (see ESI† for the comparison of traditionally aged seeding (AS) technique and the CFC-assisted impregnation seeding technique and also their subsequent secondary growth strategies). As aforementioned, when applying the conventional seeding method using aged synthesis solution (or aged seeding technique, AS), a thin layer of small ZIF-L seeds (~1.0 μm (L) × 0.5 μm (W) × 0.1 μm (H)) was formed on the inner membrane surface (Fig. 3a and inset). This is because the ageing of the seeding solution encourages small ZIF-L crystal formation in
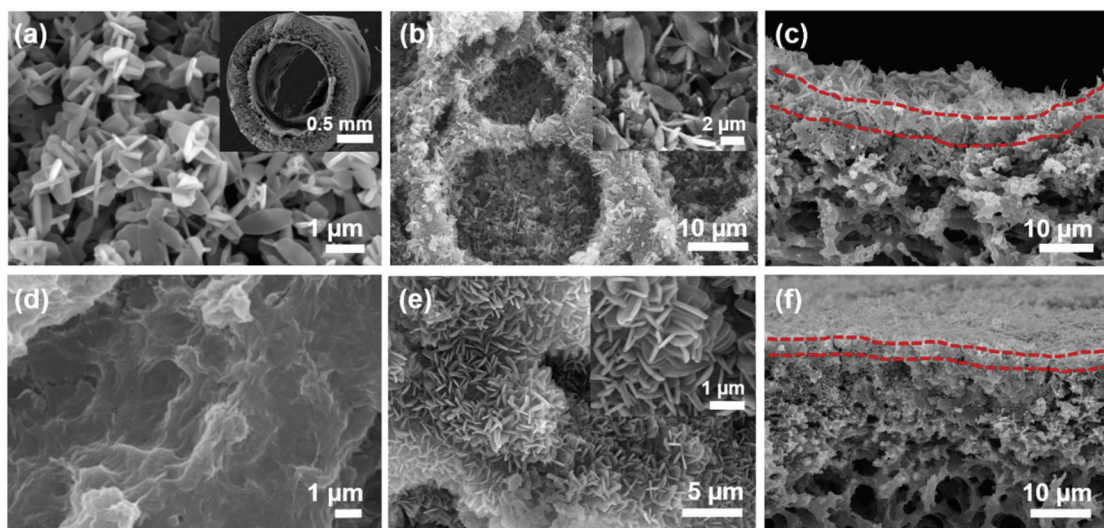

Fig. 3 SEM images of seeded hollow fibre supports and HF-ZifMs: (a) seeded surface using AS technique (inset: hollow fibre support); (b) AS HF-ZifMs (inset: close view of the membrane surface); (c) AS HF-ZifMs cross-section; (d) ligand and metal impregnated surface (L → M); (e) HF-ZifMs prepared using CFC-assisted L → M impregnation technique (inset: close view of the membrane surface); (f) cross-sectional view of HF-ZifMs prepared using CFC-assisted L → M impregnation technique.

the solution prior to the seeding procedure. These crystals were then physically deposited onto the inner membrane surface during the seeding solution circulation. After a short 50 min secondary growth at room temperature, thicker and more elongated ZIF-L crystals (3.0–7.0 μm (L) × 1–2 μm (W) × 0.3–0.8 μm (H)) were formed but still loosely packed on the surface without a preferred orientation (Fig. 3b and inset, Fig. S1†). The cross-sectional view of this hollow fibre membrane revealed that the ZIF-L layer (~10 μm in thickness) was composed of big traditional leaf-like crystals with multiple orientations (Fig. 3c). In contrast, the CFC-assisted impregnation technique significantly affected the ZIF-L crystallisation and growth orientation *via* the *in situ* formation of a dense gel layer on top of the membrane surface during the ligand → metal solution circulation steps (Fig. 3d and Fig. S2†). It has also been reported that the supersaturated gel layer usually contains abundant nuclei, which are favourably formed at the solid–liquid interface.[52,53] This thin but very dense gel layer plays a vital role in controlling the crystal size and growth orientation during the secondary growth – circulation of a recycled ligand and metal mixture solution. As shown in Fig. 3e and f, a dense layer (~4 μm) of closely packed, well inter-grown ZIF-L crystals was uniformly formed on the hollow fibre membrane support. Interestingly, the 2D ZIF-L crystals were smaller in size (2.0–4.0 μm (L) × 0.8–2.0 μm (W) × 0.3–0.5 μm (H)) as compared to those formed on a traditionally seeded membrane support. Furthermore, most leaf-like ZIF-L crystals were vertically aligned and well inter-grown on the membrane surface (Fig. 3e, inset), forming a very tight but rough ZIF-L layer with enhanced mechanical stability.

Based on the above results, the CFC-assisted impregnation seeding technique allows for the formation of a more typical seeding morphology similar to those in previous studies.[40,54] In the studies of the sequence of ligand and metal solution circulation, it was found that the formation of seeds can also be controlled by rearranging the order of ligand and metal impregnation, where applying metal impregnation prior to ligand forms larger and more evident seeds on the surface (Fig. S3†). This can be accounted for due to the 2 : 1 L : M ratio of the ZIF-L structures being more readily obtained when the ligand ratio is higher within the hollow fibre structure. Typically, the higher metal to ligand ratio in MOF synthesis solution (in our case equivalent to applying the ligand solution circulation first followed by a metal solution, L → M) favours the nucleation over the subsequent crystal growth compared to the reversed impregnation fabrication (metal solution circulation first followed by ligand solution, M → L). After circulating the ligand solution, the porous membrane support was impregnated with a limited amount of ligand solution, which can react quickly with the metal ions during the metal solution circulation, forming a thin layer of gel on the membrane surface. The remaining course of metal solution circulation thus triggered the heterogeneous nucleation in the supersaturated gel layer, which was formed at the solid–liquid interface. The favourable nucleation but low crystal growth rate can therefore be explained by the formation of a smooth gel-like

surface after impregnating metals. Thus, a thinner ZIF-L membrane with dense crystal packing and preferred orientation can be fabricated using L → M impregnation method. However, when reversing the circulation order of ligand and metal solutions, *i.e.*, M → L, similar ZIF membranes can be fabricated. The resulting membranes also showed very dense crystal packing, vertical orientation and rough surface, but the thickness was increased to 9 μm (Fig. S3d†). This is because the surface seeds were more noticeable and much bigger in size after M → L impregnation. The bigger seeds, therefore, could promote the growth of bigger ZIF crystals and thus a thicker ZIF-L membrane.

In this work, direct seeding (DS) on membrane growth was also studied. Instead of the ageing step, freshly prepared ligand and metal solutions were directly mixed and circulated in the homemade CFC system with mounted hollow fibre support, followed by 50 minutes of secondary growth with new ligand and metal mixture solution. The as-synthesised ZIF-L membranes showed much denser crystal packing and better growth orientation (Fig. S4a, b and d–f†) as compared to the samples fabricated using the ageing seeding (AS) technique which were shown in Fig. 3a–c. This further confirms that the CFC-assisted impregnation of non-aged synthesis solution facilitates more uniform and oriented growth of ZIF-L crystals on hollow fibre supports. This result is consistent with what was observed in L → M/M → L impregnation methods. However, DS and secondary growth led to the formation of a thicker ZIF-L membrane. This is because, in addition to the seeds formed at the solid and liquid interfaces, more seed crystals were deposited onto the surface during the circulation of the non-aged synthesis solution (Fig. S4c†). Unlike the L → M impregnation method, the seed formation was uncontrolled because of the presence of excess synthesis solution, leading to the growth of thicker ZIF-L coating (Fig. S4b†).

Based on the above results, the growth of ZIF-L crystals on the membrane surface differs greatly when applying different seeding techniques. The traditionally seeded membrane induced the growth of large, loosely packed crystals. However, a desirable uniformly and densely packed surface with a preferred vertical crystal orientation was achieved by the CFC-assisted impregnation technique. Additionally, the ZIF-L membrane thickness prepared using the traditionally seeded and CFC-assisted impregnated techniques was ~9 μm and ~4 μm, respectively, underscoring the latter method has significantly affected the membrane structure, surface properties and permeability which made them very promising in liquid separation (see Separation performance section below for their performance in oil/water emulsion separation).

Fine tuning of membrane surface wettability

In this study, tuning of the surface wettability of ZIF-L membranes was studied systematically. As shown in Fig. 4a (0%), the L → M ZIF-L membrane fabricated on an equivalent flat sheet porous nylon support under the same synthesis conditions showed an initial water contact angle of ~82° which quickly decreased to 0° in about 4 s. Note that some of the
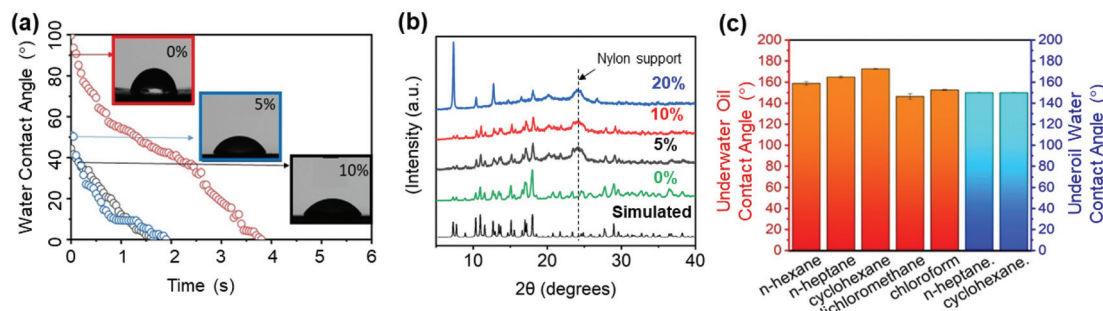
Fig. 4 Surface characterisations; (a) dynamic water contact angle measurements, (b) XRD analysis and (c) underoil water contact angle and underwater oil contact angle measurements of HF-ZifMs prepared using CFC-assisted L → M impregnation technique and different ethanol contents.

ZIF-L membranes in this single study were fabricated on an equivalent flat sheet porous nylon support (Whatman, 500 nm pore size) to represent the ZIF coating on the internal hollow fibre membrane surface and also to better characterise their surface properties, such as surface wettability, using kinetic water contact angle measurements. When simply adding a co-solvent (e.g., ethanol) during the secondary membrane growth, similar ZIF membranes can be prepared for these L → M HF-ZifMs. More interestingly, their surface wettability can be finely tuned by controlling the co-solvent content in the synthesis solution. In this work, 0–20% V/V ethanol was studied, and a range of ZIF membranes was fabricated both on flat sheet and hollow fibre membrane supports. When the content of ethanol was controlled under 10% V/V in the system, pure ZIF-L coated membranes were synthesised with characteristic leaf-like morphology (Fig. S5a–f†). The increase of ethanol content was found to slightly impact the crystal morphology and surface roughness. More ethanol in the solution favours crystals with reduced lateral size and increased thickness, however, retaining pure ZIF-L structure (Fig. 4b, simulated, 5% and 10%) (see Fig. S5 and S6† for further SEM images of hollow fibre supported ZIF-L membranes fabricated using AS, DS, or M → L/L + M impregnation seeding techniques with/without ethanol).[55–57] Conversely, 20% V/V ethanol demonstrated larger crystal impurities with a more predominant peak associated with a characteristic ZIF-8 structure (Fig. 4b, 20%). Based on the morphology it can be deduced that 20% V/V ethanol produced very small and thick crystals which were uniformly packed on the surface (Fig. S7†). Based on the formation of ZIF-8 with equivalent metal and ligand concentrations within an alcohol environment, it can be deduced that ethanol directly affects the crystal morphology.[58,59] Furthermore, the solvent has proven to have phase transformation abilities (ZIF-L to ZIF-8),[60] suggesting a potential preference for the formation of the 3D isomeric equivalent. Overall, the formation of ZIF-8 in ethanol environments can account for the formation of shorter and thicker crystals which decrease the surface roughness.

The dynamic water contact angle (WCA) in Fig. 4a confirmed that the surface hydrophilicity of the ZIF-L membranes prepared with ethanol could be significantly improved by increasing the ethanol content from 0% to 5%–10% V/V. This phenomenon was further evidenced in each fabrication approach, with all of the HF-ZifMs exhibiting improved surface hydrophilicity as ethanol content increased to 10% V/V (Fig. S8†). More specifically L → M HF-ZifM's initial water contact angle was reduced from ~80° for 0% V/V ethanol to ~65° for 5% V/V ethanol and then to ~50° for 10% V/V ethanol. The water droplet rapidly spreads on the surface in only 2 s and 1.7 s for 5% V/V and 10% V/V ethanol contents, respectively, suggesting the presence of low quantities of ethanol attributes to the superhydrophilic and highly permeable nature of the ZIF-L membranes in air. Likewise, the underwater oil contact angles and underoil water contact angles were measured to evaluate the surface property of the as-synthesised ZIF-L membranes. 5 types of oils were used for the underwater oil contact angle and underoil water contact angle measurements, and their results were shown in Fig. 4c. During the measurements, most oils/water droplet maintained a quasi-spherical shape on the membrane surface with a contact angle larger than 150° (for example, cyclohexane displayed the high underwater oil contact angle of ~170°), confirming the underwater superoleophobic and underoil superhydrophobic nature of the ZIF-L membranes synthesised in the presence of ethanol (see Fig. S9† for underwater oil contact angle and underoil water contact angle measurements).

It has been reported that both chemical composition/surface energy and surface roughness contribute to surface wetting properties.[61] In terms of ZIF-L, the materials coordination bond, hydrophilic Zn^{2+} centres and high energy imidazolate linkers create a high surface energy and, in turn, a hydrophilic material.[62,63] Such hydrophilic surfaces have previously been described by the Wenzel model, stating the surface hydrophilicity will increase with surface roughness due to capillary effects. Hence the unique wettability properties of the ZIF-L membranes prepared with ethanol can be attributed to both the surface roughness, which is enhanced by the ethanol presence, and the hydrophilic nature of the ZIF-L crystals. Notably, the presence of ethanol during secondary membrane growth significantly increased the hydrophilicity and wettability of the surface (Fig. 4a and Fig. S8†). To ensure the

successful replication of the optimum ZIF-L structures and surface properties on hollow fibre membrane supports which were previously seeded *via* AS, DS or the CFC-assisted L → M/M → L impregnation, the same amount of ethanol (10% V/V) was thoroughly mixed with the recycled ligand and metal mixture solutions, followed by a short secondary membrane growth using the CFC-assisted synthesis method. It's worthwhile mentioning that the resulting hollow fibre supported ZIF-L membranes showed very similar surface crystal packing, orientation and surface roughness to those of ZIF-L membranes prepared previously without involving ethanol (Fig. S5 and S6†).

Oil/water emulsion separation performance

As aforementioned, seeding techniques, membrane morphology and surface wettability play crucial roles in liquid separations. In this study, all ZIF-L membranes prepared using different seeding techniques and secondary growth methods with or without ethanol were tested for water remediation from a series of oil-in-water emulsions. Their oil rejection performance was evaluated in a homemade continuous crossflow system with a fixed internal pressure of 1 bar. The removal of water from a surfactant stabilised cyclohexane-in-water emulsion is illustrated in Fig. 5 with the water permeation occurring from the internal to the external surface of the hollow fibre membrane.

First, the flux and separation efficiency of all as-synthesised hollow fibre supported membranes prepared using different seeding techniques (including aged seeding (AS), direct seeding (DS), M → L impregnation and L → M impregnation) were studied and compared to that of the bare hollow fibre membrane. According to the results shown in Fig. 6a (cyclohexane-in-water emulsion separation), the bare hollow fibre membrane support only exhibited an oil rejection of ~35% and a water flux of ~410 L m^{-2} h^{-1} bar^{-1} using the homemade continuous crossflow separation system. After the ZIF-L growth, all membranes prepared using different seeding techniques (except samples fabricated using DS + 5% V/V ethanol and AS + 5% V/V ethanol) showed a significantly increased oil rejection rate of >99%, indicating the rough ZIF-L coating was

effective for water remediation from emulsified oily wastewater.

However, ZIF-L membranes that were prepared using the CFC-assisted L → M/M → L impregnation methods exhibited an overall higher clean water production (485–>1300 L m^{-2} h^{-1} bar^{-1}), attributed to the thinner, rougher and more orientated features of the surface ZIF-L coating. Additionally, when increasing the ethanol content during the secondary growth, all the resulting membranes (except samples fabricated using DS + 5% V/V ethanol and AS + 5% V/V ethanol) showed dramatically increased water permeance (>700 L m^{-2} h^{-1} bar^{-1}). For instance, the membrane fabricated using L → M impregnation and 10% V/V ethanol showed the highest water flux of ~1300 L m^{-2} h^{-1} bar^{-1} whilst maintaining a high oil rejection rate (~99.9%), which is much higher than that of bare hollow fibre support (~410 L m^{-2} h^{-1} bar^{-1}) and the membranes prepared using conventional AS and DS techniques (200–780 L m^{-2} h^{-1} bar^{-1}). This is because the surface ZIF-L coating consists of smaller but more oriented crystals, thus forming much larger channels/pores for easier and faster water permeation.

Furthermore, this membrane (L → M impregnation and 10% V/V ethanol) demonstrated an excellent rejection rate for various oils, for example, cyclohexane (99.8%), *n*-hexane (99.4%), *n*-heptane (99.8%), chloroform (99.9%), and dichloromethane (98.8%), whilst maintaining a high water flux (820–1310 L m^{-2} h^{-1} bar^{-1}) (Fig. 6b). As reported previously, the lower density oils reduced the flux in comparison to denser oils.[36] To study the mixture oil rejection performance, two types of oil mixture emulsions were prepared with one solely consisting of lower density oils (mix 1: cyclohexane, *n*-hexane and *n*-heptane in water (1:1:1:297 V/V%)) and another with a mixture of heavy oils (mix 2: chloroform and dichloromethane in water (1:1:198 V/V%)). As shown in Fig. 6b, the membranes maintained a separation efficiency >98.5% for both oil mixtures, however, with lower flux (~820 L m^{-2} h^{-1} bar^{-1}) for the lower density oil mixture and greater flux rates presented with the presence of higher density oils (~1285 L m^{-2} h^{-1} bar^{-1}).

Photos of the feed and permeate after the separation of different oil emulsions (*n*-hexane/water, *n*-heptane/water,
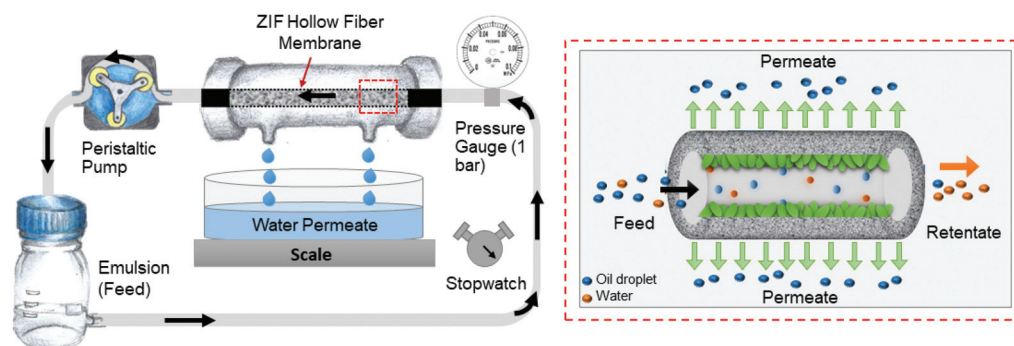

Fig. 5 Pure water and O/W emulsion separation process: schematic illustration of separation apparatus (on left-hand side) and separation mechanism (on right-hand side).
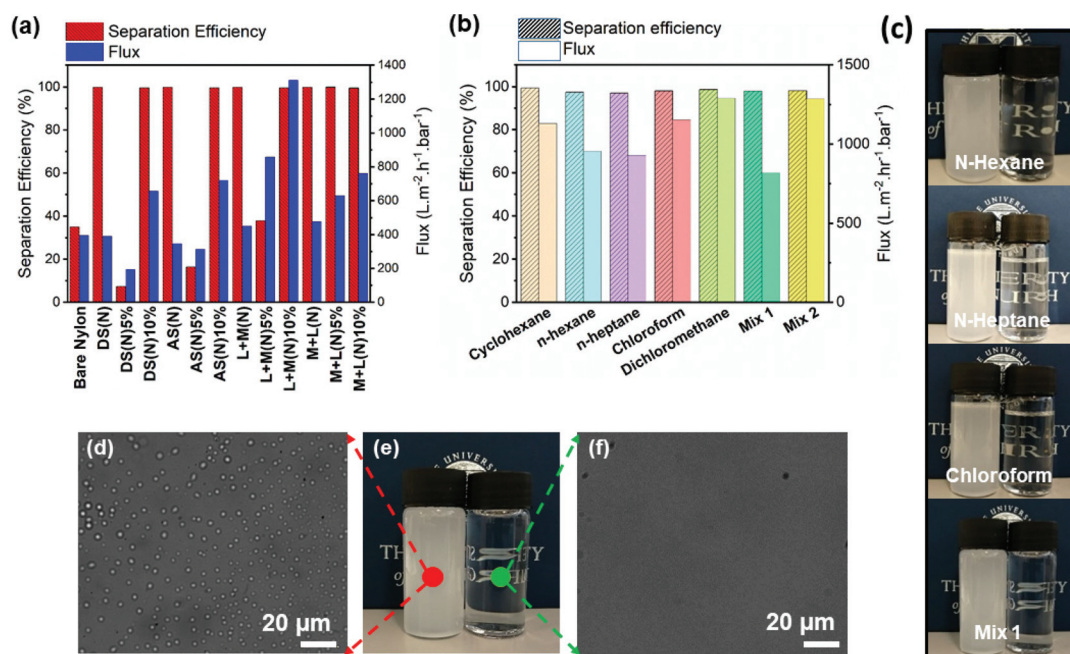
Fig. 6   Separation efficiency of HF–ZifMs prepared using different seeding techniques and ethanol contents; (a) oil-in-water emulsion separation performance; (b) separation efficiency (oil rejection rate) and flux for various oils; (c) photographic imaging of feed and filtrate for various oil-in-water emulsions; (d) microscopic imaging of cyclohexane emulsion feed; (e) photographic image of feed and filtrate for cyclohexane emulsion; (f) microscopic imaging of cyclohexane emulsion filtrate.

chloroform/water and oil mixture/water emulsion 1) *via* L → M impregnated membrane were highlighted in Fig. 6c. Specifically, the milky emulsions on the left-hand side have been significantly clarified after passing the hollow fibre membrane (on the right-hand side). Fig. 6d–f showed its separation result of Tween80-stabilised cyclohexane-in-water emulsion. Comparison of the optical microscopy images reveals the substantial difference in the phase compositions between the initial cyclohexane-in-water emulsion and the corresponding permeate. The emulsion image highlights the high volume of oil droplets within the solution (Fig. 6d). After the separation process, there are no visible droplets observed in the sample (Fig. 6f). See Videos S1 and S2 in ESI† for more details.

According to Table S1,† previous hollow fibre membranes showed a water flux up to 900 L m^{-2} h^{-1} bar^{-1} and an oil rejection rate up to 99.9%, revealing the excellent separation performance of the ZIF-L coated hollow fibre membrane presented in this work. This can be attributed to both the physical and chemical properties of the membrane, the hydrophilicity of ZIF-L, the thin active layer and the high surface area to volume ratio of the hollow fibre membrane.

Antifouling property

It has been known that the antifouling properties on the nanostructured surfaces might be further improved by achieving superamphiphobicity – an effect where surface roughness and surface chemistry combine to generate surfaces that are both superhydrophobic and superoleophobic.[59] The hollow fibre supported ZIF membranes fabricated in this work, particularly

membranes synthesised using L → M impregnation seeding technique, displayed unique roughness, giving underoil superhydrophobicity and underwater superoleophobicity. To examine their anti-fouling property, extended pure water and oil/water emulsion separation were carried out for up to 120 minutes and 30 minutes, respectively. The tests were undertaken at equivalent conditions as the emulsion separation (*i.e.*, continuous crossflow separation at 1 bar pressure). In pure water permeation tests, as shown in Fig. 7a, the ZIF-L-coated membrane demonstrated a significantly improved water flux rate than the bare hollow fibre membrane. The increased flux rate underscored a lower self-fouling property of the ZIF-L membranes.

Similarly, real-time cyclohexane-in-water emulsion separation on the as-synthesised membranes fabricated using different seeding techniques was studied. All membranes showed higher initial water flux at the beginning (Fig. 7b). According to the results, DS, AS and M → L membranes required more than 15 min to achieve a stable water flux (~360 L m^{-2} h^{-1} bar^{-1}). While L → M membrane showed a much higher initial water flux (~1400 L m^{-2} h^{-1} bar^{-1}) which was then quickly stabilised at ~1150 L m^{-2} h^{-1} bar^{-1} in less than 3 min, indicating that the thinner ZIF-L coating with uniform crystal packing and orientation on L → M membrane significantly improves the water permeation and, more importantly, the antifouling/self-cleaning property of its surface structure. These results are consistent with those reported in one of our earlier studies.[46] Moreover, Fig. 7c highlights the advantages of using ethanol during fabrication. The more ethanol (in the
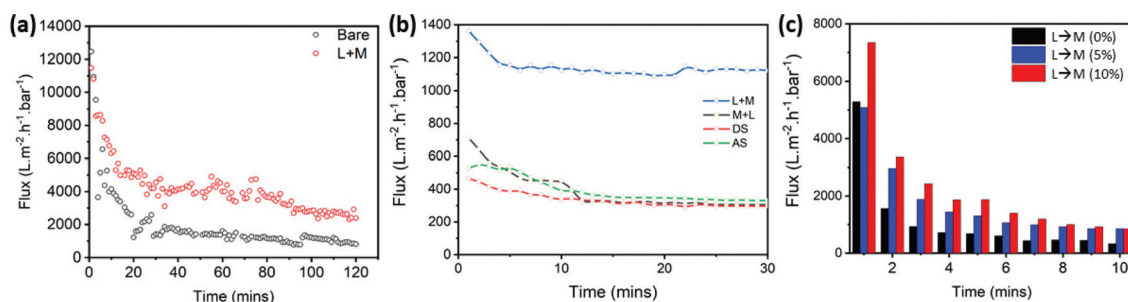
Fig. 7 Membrane anti-fouling properties: (a) pure water permeation; (b) oil-in-water emulsion separation; (c) effect of ethanol content on membrane permeate flux.

range of 0%–10% V/V) was added, the higher water flux was observed, demonstrating further increased self-cleaning property and reduced fouling. This can be explained by the increased packing density/roughness and smaller crystals and hence the reduction in the intracrystal voids available for oil droplets to contaminate. Therefore, it can be concluded that the impregnation of ligand then metal can improve the membrane flux and antifouling properties based on the control of crystal size, growth orientation and packing/alignment density with ethanol, further improving the hydrophilicity and underwater superoleophobicity.

To validate the newly designed CFC-assisted impregnation and secondary membrane formation methods, the growth of another type of MOF material, ZIF-8, on the hollow fibre supports was also studied. See Fig. S10† for the details of this study and the discussion on the characterisation results and separation performance of the as-synthesised ZIF-8 hollow fibre membranes. Overall, the continuous fluid circulation technique proposed in this work was of great importance in controlling the crystal formation on hollow fibre membrane supports and provided a faster, more controllable and sustainable secondary membrane growth method by using the recycled expensive ligand and metals solutions. The as-synthesised ZIF-L membranes with unique surface structures showed superhydrophilic, ultra permeable and underwater superoleophobic properties, which are crucial in ultrafast water remediation from challenging oil/water emulsions.

Hydrochemical stability

Besides the flux and separation efficiency, the hydrochemical stability and recyclability of the membrane are also very important in any liquid separation, *e.g.*, oil/water separation. It is of particular interest to maintain the membrane performance in harsh environments for actual oil/water mixture separation. ZIF materials are typically considered to have a relatively low hydrochemical stability.[64,65] It has been reported that the leaf-like ZIF-L crystals can be destroyed/amorphized in several minutes when they are in full contact with water under a strong scanning electron beam.[66] This is due to the stability being dependant on the relatively weak metal to ligand bond strength as well as the weak hydrogen bonds between crys-

tals.[67] To analyse this effect on the membrane performance, the membranes were continually exposed to water and subjected to different pHs over different periods.

Fig. 8 highlights crystal morphological change of ZIF-L membrane after 12 hours soaking in aqueous solutions with different pHs and 12 hours in pure water. As shown in Fig. 8b and e, ZIF-L membranes exposed to both mild acid (pH = 5) and base (pH = 9) solutions showed an interesting morphological adaptation to more spherical crystals without substantial degradation. High-magnification SEM images showed these were stacks of thin ZIF-L nanosheets (Fig. 8b, inset and e, inset). This is attributed to the increased dissolution rate of the crystals in slightly lower and higher pH environments and hence a lower membrane coverage with the stacked ZIF-L crystals. In contrast, after soaking in a highly basic solution (pH = 11) and strong acid solution (pH = 3), most surface crystals were destroyed and became smaller and thinner (Fig. 8c and f, insets), suggesting their lower structure stability under these harsh conditions. Surprisingly, unlike the results reported elsewhere,[68] the ZIF-L membranes (fabricated using the L → M impregnation method) demonstrated promising hydrochemical stability with a minimum morphological change up to 12 hours (Fig. 8d and Fig. S11†). After 12 hours of pure water treatment, the resultant membrane exhibited similar crystallinity to the initial sample (Fig. S12†), maintaining 95.09% of its initial ZIF load (Zif-wt%) incorporated in the HF-ZifM. The significantly improved hydrochemical stability of the ZIF-L membranes is attributed to the close packing/alignment of the leaf-like crystals with similar orientations, which could protect the crystals from water attack. However, further submersion (>36 h) in water induces significant amorphization, reducing the ZIF load by 35.52 Zif-wt%, and a possible recrystallisation process, forming materials with larger multidirectional geometries (Fig. S11 and S12†).

The oil/water separation performance of ZIF-L membranes after exposure to different acidic/basic solutions over various time intervals up to 12 hours (2, 4, 8 and 12 hours) was then studied in detail. As shown in Fig. 8g and h, acid and alkaline post-treatment influenced both the flux and the separation efficiency. The membrane samples showed dramatically increased flux from >1300 to ~8000 L m^{-2} h^{-1} bar^{-1} and decreased oil rejection rate from ~99.9% to ~77.6% when
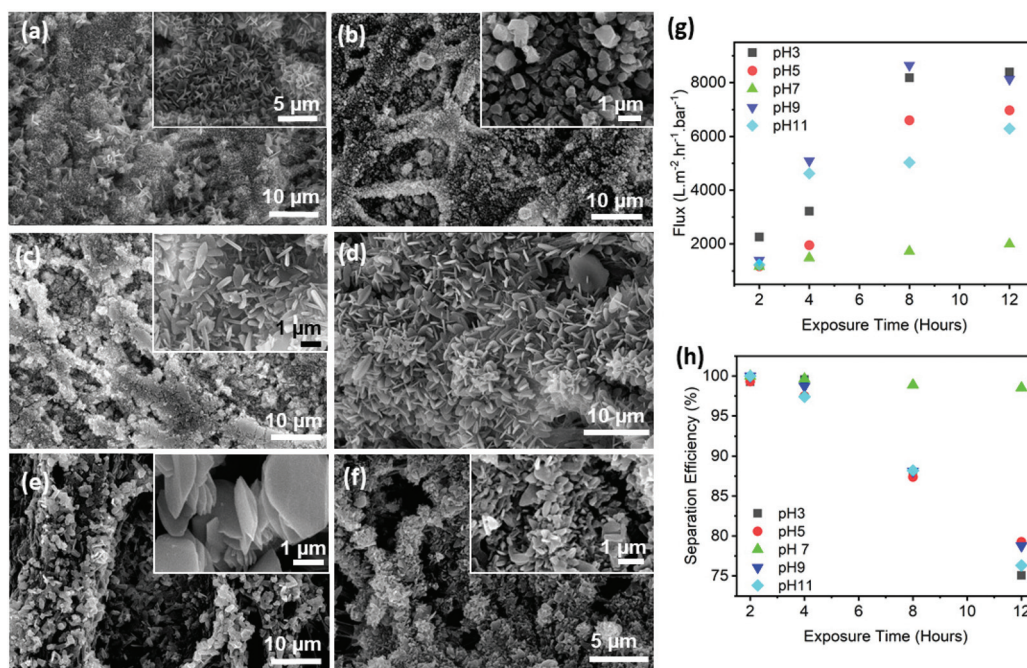
Fig. 8 Stability analysis of HF–ZifMs prepared using CFC-assisted L → M impregnation technique and 10% V/V ethanol. SEM images of (a) initial membrane surface before acid/alkaline post-treatments, (b) after 4 hours exposure to pH 9, (c) after 4 hours exposure to pH 11, (d) after 12 hours exposure to water, (e) after 4 hours exposure to pH 5, and (f) after 4 hours exposure to pH 3; and (g) permeate flux after pH chemical exposure; (h) separation efficiency (oil rejection rate) after pH chemical exposure. Insets: high-magnification SEM images of the membrane surface.

treated in harsher conditions (*i.e.*, higher/lower pH and/or longer soaking time). This is due to the collapse of surface ZIF-L packing and the degradation of crystalline structures, leading to the formation of more unselective and big pores/channels for oily mixture permeation. It's worthwhile mentioning that the membranes post-treated by acid solutions showed worse separation efficiency, as indicated by the higher flux and lower oil rejection rate, as compared with those of alkaline treated membrane. Despite the decrease in separation performance, the membranes still demonstrate a greater separation than bare PES membrane. This may be attributed to the presence of ZIF-L crystals within the porous structure. However, the membrane after 12 h pure water treatment showed almost intact structures (Fig. 8d) and similar separation performance, *i.e.*, a slight increase in the water flux (from ~1150 to ~2, 000 L m^{-2} h^{-1} bar^{-1}) and a minor influence on the oil rejection rate (from 99.9% to 98.0%). These results further confirm that the unique surface structures of the as-synthesised ZIF membranes played a crucial role in ultrafast water transport.

Conclusion

In conclusion, a facile continuous fluid circulation method has been proposed in this study to fabricate uniformly oriented ZIF-L crystals on the internal surface of hollow fibres under ambient conditions. The new seeding technique – CFC-assisted impregnation of ligand then metal solution – was

found to greatly impact the separation performance of the membrane due to changes in both physical and chemical properties. This simple impregnation technique promotes the formation of a thin gel-like seed layer with abundant nuclei islands which was found to improve the crystal packing/orientation, surface wettability and oil/water emulsion separation efficiency of the resulting membranes. Furthermore, this fabrication method is facile and more environmentally friendly by using recycled synthesis solutions with a reduced volume of waste. Overall, the fabrication route reported in the present work is of great potential in the rapid and economical mass production of self-cleaning ZIF-L based hollow fibre materials for ultrafast continuous oil-in-water emulsion separations.

Conflicts of interest

The authors declare there are no conflicts of interest.

Acknowledgements

Notes and references

1 W. Zhang, N. Liu, Y. Cao, Y. Chen, L. Xu, X. Lin and L. Feng, *Adv. Mater.*, 2015, **27**, 7349–7355.

2 T. Oki and S. Kanae, *Science*, 2006, **313**, 1068–1072.

3 M. A. Shannon, P. W. Bohn, M. Elimelech, J. G. Georgiadis, B. J. Marĩas and A. M. Mayes, *Nature*, 2008, **452**, 301–310.

4 K. Bouchemal, S. Briançon, E. Perrier and H. Fessi, *Int. J. Pharm.*, 2004, **280**, 241–251.

5 B. A. Khan, N. Akhtar, H. M. S. Khan, K. Waseem, T. Mahmood, A. Rasul, M. Iqbal and H. Khan, *Afr. J. Pharm. Pharmacol.*, 2011, **5**, 2715–2725.

6 M. M. Abdulredha, H. Siti Aslina and C. A. Luqman, *Arabian J. Chem.*, 2020, **13**(1), 3403–3428.

7 E. Dickinson, *Food Hydrocolloids*, 2009, **23**, 1473–1482.

8 Y. Yamashita, R. Miyahara and K. Sakamoto, *Cosmet. Sci. Technol. Theory Princ. Appl.*, 2017, 489–506.

9 L. Ben Mansour and S. Chalbi, *J. Appl. Electrochem.*, 2006, **36**, 577–581.

10 Y. O. Fouad, *Alexandria Eng. J.*, 2014, **53**, 199–204.

11 A. Y. Hosny, *Sep. Technol.*, 1996, **6**, 9–17.

12 Y. Si, Q. Fu, X. Wang, J. Zhu, J. Yu, G. Sun and B. Ding, *ACS Nano*, 2015, **9**, 3791–3799.

13 M. Tir and N. Moulai-Mostefa, *J. Hazard. Mater.*, 2008, **158**, 107–115.

14 R. K. Gupta, G. J. Dunderdale, M. W. England and A. Hozumi, *J. Mater. Chem. A*, 2017, **5**, 16025–16058.

15 T. Turken, R. Sengur-Tasdemir, E. Ates-Genceli, V. V. Tarabara and I. Koyuncu, *J. Water Process Eng.*, 2019, **32**, 100938.

16 J. Li, S. Yuan, J. Wang, J. Zhu, J. Shen and B. Van der Bruggen, *J. Membr. Sci.*, 2018, **553**, 139–150.

17 P. Janknecht, A. D. Lopes and A. M. Mendes, *Environ. Sci. Technol.*, 2004, **38**, 4878–4883.

18 J. H. Jhaveri and Z. V. P. Murthy, *Desalination*, 2016, **379**, 137–154.

19 R. D. Noble, *Sep. Sci. Technol.*, 1987, **22**, 731–743.

20 Z. Chu, Y. Feng and S. Seeger, *Angew. Chem., Int. Ed.*, 2015, **54**, 2328–2338.

21 O. S. H. Santos, M. C. da Silva and M. I. Yoshida, *J. Appl. Polym. Sci.*, 2017, **134**, 1–8.

22 X. Feng and L. Jiang, *Adv. Mater.*, 2006, **18**, 3063–3078.

23 Z. Xue, Y. Cao, N. Liu, L. Feng and L. Jiang, *J. Mater. Chem. A*, 2014, **2**, 2445–2460.

24 T. Chen, M. Duan and S. Fang, *Ceram. Int.*, 2016, **42**, 8604–8612.

25 H. Shao, Y. Qi, J. Cheng and S. Qin, *React. Funct. Polym.*, 2019, **143**, 104330.

26 X. Zhu, W. Tu, K. H. Wee and R. Bai, *J. Membr. Sci.*, 2014, **466**, 36–44.

27 H. Wang, X. Hu, Z. Ke, C. Z. Du, L. Zheng, C. Wang and Z. Yuan, *Nanoscale Res. Lett.*, 2018, **13**, 284.

28 D. Cheng, L. Zhao, N. Li, S. J. D. Smith, D. Wu, J. Zhang, D. Ng, C. Wu, M. R. Martinez, M. P. Batten and Z. Xie, *J. Membr. Sci.*, 2019, **588**, 117204.

29 J. Li, Y. Labreche, N. Wang, S. Ji and Q. An, *Chin. J. Chem. Eng.*, 2019, **27**, 2376–2382.

30 B. Wang, A. P. Côté, H. Furukawa, M. O'Keeffe and O. M. Yaghi, *Nature*, 2008, **453**, 207–211.

31 K. Tao, L. Cao, Y. Lin, C. Kong and L. Chen, *J. Mater. Chem. A*, 2013, **1**, 13046–13049.

32 K.-Y. Andrew Lin and H.-A. Chang, *J. Mater. Chem. A*, 2015, **3**, 20060–20064.

33 S. S. Sankar, S. R. Ede, S. Anantharaj, K. Karthick, K. Sangeetha and S. Kundu, *Catal. Sci. Technol.*, 2019, **9**, 1847–1856.

34 S. Yuan, J. Zhu, Y. Li, Y. Zhao, J. Li, P. V. Puyvelde and B. V. D. Bruggen, *J. Mater. Chem. A*, 2019, **7**, 2723–2729.

35 Y. Cai, D. Chen, N. Li, Q. Xu, H. Li, J. He and J. Lu, *J. Membr. Sci.*, 2017, **543**, 10–17.

36 H. Li, L. Zhu, J. Zhang, T. Guo, X. Li, W. Xing and Q. Xue, *Appl. Surf. Sci.*, 2019, **476**, 61–69.

37 D. Qin, Z. Liu, H. Bai, D. D. Sun and X. Song, *Sci. Rep.*, 2016, **6**, 1–12.

38 S. Xu, L. F. Ren, Q. Zhou, H. Bai, J. Li and J. Shao, *J. Appl. Polym. Sci.*, 2018, **135**, 1–9.

39 C. Ma, Y. Li, P. Nian, H. Liu, J. Qiu and X. Zhang, *Sep. Purif. Technol.*, 2019, **229**, 115835.

40 Q. Gu, N. T. C. Albert, Q. Sun, A. M. K. Elshahawy, Z. Lyu, Z. He, L. Zhang, H. Y. Ng, K. Zeng and J. Wang, *RSC Adv.*, 2019, **9**, 1591–1601.

41 C. Wang, Y. V. Kaneti, Y. Bando, J. Lin, C. Liu, J. Li and Y. Yamauchi, *Mater. Horiz.*, 2018, **5**, 394–407.

42 F. Zhang, J. Dou and H. Zhang, *Polymers*, 2018, **10**, 1340.

43 P. Krzeminski, J. A. Gil, A. F. V. Nieuwenhuijzen, J. H. J. M. van der Graaf and J. B. V. Lier, *Desalin. Water Treat.*, 2012, **42**, 100–106.

44 X. R. Zhang, T. Liu, L. Braeken, Z. Liu, X. L. Wang and B. V. D. Bruggen, *J. Appl. Polym. Sci.*, 2015, **132**, 1–9.

45 P. M. Doran, *Bioprocess Eng. Princ.*, 2013, 445–595.

46 T. Chen, A. Lewis, Z. Chen, X. Fan, N. Radacsi, A. J. C. Semiao, H. Wang and Y. Huang, *Sep. Purif. Technol.*, 2020, **240**, 116647.

47 Z. Xiong, H. Lin, F. Liu, P. Xiao, Z. Wu, T. Li and D. Li, *Sci. Rep.*, 2017, **7**, 1–12.

48 N. Rangnekar, N. Mittal, B. Elyassi, J. Caro and M. Tsapatsis, *Chem. Soc. Rev.*, 2015, **44**, 7128–7154.

49 Y. Lo and D. Y. Kang, *J. Mater. Chem. A*, 2016, **4**, 4172–4179.

50 Z. Zhong, J. Yao, R. Chen, Z. Low, M. He, J. Z. Liu and H. Wang, *J. Mater. Chem. A*, 2015, **3**, 15715–15722.

51 X. Li, Y. Liu, J. Wang, J. Gascon, J. Li and B. V. D. Bruggen, *Chem. Soc. Rev.*, 2017, **46**, 7124–7144.

52 Y. Huang, D. Dong, J. Yao, L. He, J. Ho, C. Kong, J. A. Hill and H. Wang, *Chem. Mater.*, 2010, **22**, 5271–5278.

53 Y. Huang, J. Yao, X. Zhang, C. Kong, H. Chen, D. Liu, M. Tsapatsis, R. M. Hill, J. A. Hill and H. Wang, *CrystEngComm*, 2011, **13**, 4714–4721.

54 J. Zhu, H. Li, J. Hou, J. Liu, Y. Zhang and B. V. D. Bruggen, *AIChE J.*, 2020, **66**, 1–9.

55 A. M. Nasir, N. A. H. Md Nordin, P. S. Goh and A. F. Ismail, *J. Mol. Liq.*, 2018, **250**, 269–277.

56 G. Liu, Z. Jiang, K. Cao, S. Nair, X. Cheng, J. Zhao, H. Gomaa, H. Wu and F. Pan, *J. Membr. Sci.*, 2017, **523**, 185–196.

57 J. Zhang, T. Zhang, D. Yu, K. Xiao and Y. Hong, *CrystEngComm*, 2015, **17**, 8212–8215.

58 H. J. Lee, W. Cho and M. Oh, *Chem. Commun.*, 2012, **48**, 221–223.

59 V. Vatanpour and S. Khorshidi, *Mater. Chem. Phys.*, 2020, **241**, 122400.

60 H. Fu, Z. Wang, X. Wang, P. Wang and C. Wang, *CrystEngComm*, 2018, **20**, 1473–1477.

61 Y. Coffinier, G. Piret, M. R. Das and R. Boukherroub, *C. R. Chim.*, 2013, **16**, 65–72.

62 A. U. Ortiz, A. P. Freitas, A. Boutin, A. H. Fuchs and F. Coudert, *Phys. Chem. Chem. Phys.*, 2014, **16**, 9940–9949.

63 R. Chen, J. Yao, Q. Gu, S. Smeets, C. Baerlocher, H. Gu, D. Zhu, W. Morris, O. M. Yaghi and H. Wang, *Chem. Commun.*, 2013, **49**, 9500–9502.

64 Z. Chu and S. Seeger, *Chem. Soc. Rev.*, 2014, **43**, 2784–2798.

65 W. Shi, X. Liu, C. Ye, X. Cao, C. Gao and J. Shen, *Sep. Purif. Technol.*, 2019, **210**, 885–890.

66 K. S. Park, Z. Ni, A. P. Cote, J. Y. Choi and R. Huang, *Proc. Natl. Acad. Sci. U. S. A.*, 2006, **103**, 10186–10191.

67 S. Conrad, P. Kumar, F. Xue, L. Ren, S. Henning, C. Xiao, P. K. A. Mkhoyan and P. M. Tsapatsis, *Angew. Chem., Int. Ed.*, 2018, **57**, 13592–13597.

68 Y. Lo, C. H. Lam, C. W. Chang, A. C. Yang and D. Y. Kang, *RSC Adv.*, 2016, **6**, 89148–89156.